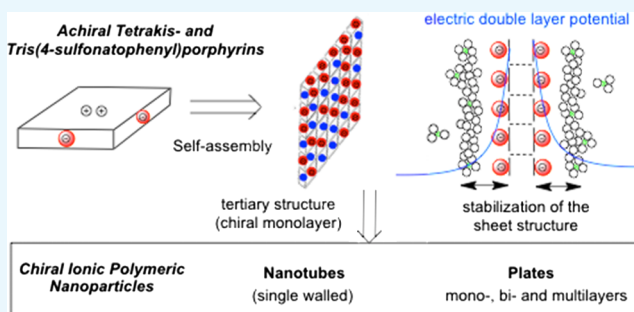# Diastereoisomerism, Stability, and Morphology of Substituted *meso*-4-Sulfonatophenylporphyrin J-Aggregates

Zoubir El-Hachemi,[*,†,‡] Joaquim Crusats,[†,‡] Carlos Troyano,[†] and Josep M. Ribó[†,‡]

†Department of Inorganic and Organic Chemistry, Organic Chemistry Section, University of Barcelona, C. Martí i Franquès 1, E-08028 Barcelona, Catalonia, Spain

‡Institute of Cosmos Science, Universitat de Barcelona (IEEC-ICC), C. Martí Franquès 1, E-08028 Barcelona, Catalonia, Spain

**S** Supporting Information

**ABSTRACT:** The comparison between nanoparticle morphologies of the J-aggregates of different *meso*-4-sulfonatophenylporphyrins showing non-sulfonato groups at some of the *meso*-positions constitutes an ultimate proof of the 2D crystal-like character of the basic self-assembly motif of this family of J-aggregates. Diastereoisomerism stemming from the tacticity of the relative configurations in relation to the J-aggregate bidimensional sheet is the key factor that determines both the striking monolayer in solution and also the hierarchical pathways leading to different nanoparticle morphologies upon further growth. The unexpected stability of such large monolayered sheets made up of porphyrin units is probably caused by the support originated at both surface faces by the double layer potentials of the peripheral ionic substituents. These double layer potentials play a driving role in the subsequent 3D growth of the monolayers, as deduced herein from the determining role of tacticity both in the stability of the J-aggregate sheet and in its evolution either to monolayered or to bilayered nanoparticles. The stabilizing role of the forces at the electrical double layer of the particle suggests a relationship between these forces and the previously reported detection of racemic biases when shear hydrodynamic forces are in action during the aggregation process.

Achiral Tetrakis- and Tris(4-sulfonatophenyl)porphyrins

electric double layer potential

Self-assembly

tertiary structure (chiral monolayer)

stabilization of the sheet structure

Chiral Ionic Polymeric Nanoparticles | Nanotubes (single walled) | Plates mono-, bi- and multilayers

## INTRODUCTION

Amphiphilic porphyrin J-aggregates have a wide range of potential applications (e.g., refs[1−3]). However, there is still a lack of knowledge about the self-assembly pathways of the hierarchical aggregation process that determine the inner structure of these aggregates and their nanoparticle morphology[4−7] and, consequently, about the experimental conditions leading to homogeneous nanoparticle samples. Recent reports on the competing interactions in the self-assembly of these type of compounds show the complexity of such a hierarchical self-assembly.[8−10]

The case of the meso-substituted 4-sulfonatophenyl-and-aryl-substituted porphyrins leading to J-aggregates, when the inner core of the porphyrin ring is diprotonated, is now a paradigm of hierarchical self-assembly. On the basis of the previous reports (e.g., refs[7−10]), we distinguish between two phases of the aggregation process: (a) the initial self-assembly yielding a 2D ionic polymer of quite a specific structure and; (b) the evolution of this secondary structure to nanoparticles of diverse morphologies.

In respect to (a), all experimental evidence suggest that self-assembly polymerization is a process showing similarities to that of crystal nucleation; to an initial endergonic isodesmic polymerization, a cooperative polymerization follows once a critical size cluster has been reached, changing the growth

dynamics to an exergonic one.[11] Diffraction data of the J-aggregates of achiral $H_2TPPS_4^{2-}$ (Scheme 2) show that the self-assembled structure is a chiral sheet of an ionic polymer formed by the edge-to-edge and face-to-face interactions of the amphiphilic monomeric zwitterions, stabilized by hydrogen bonding interactions and by hydrophobic effects (Scheme 1).[12] This sheet is formed by pairs of conformationally racemic dimers showing an alternate twist along the vertical axis (y, Scheme 1) and a distortion out of the x,y-plane, which, on the whole, leads to an intrinsically chiral structure ($P2_1$). As most often occurs in many supramolecular self-assembly structures, this initial 2D crystallization-like process cannot progress to the formation of crystal 3D structures, that is, further grow along the axis z of Scheme 1. J-aggregates of derivatives of all substituted 4-sulfonatophenylporphyrins reported herein show similar electronic spectra than those of $H_2TPPS_4^{2-}$ J-aggregates.[7,12] This suggests a common fundamental self-assembly structure for all the J-aggregates of this family of diprotonated amphiphilic porphyrins. However, when one of the mesosubstituents is not a 4-sulfonatophenyl group, then

**Scheme 1. Primordial Chiral Sheet of $H_2TPPS_4^{2-}$ J Aggregates (One Enantiomorph Represented)[a]**
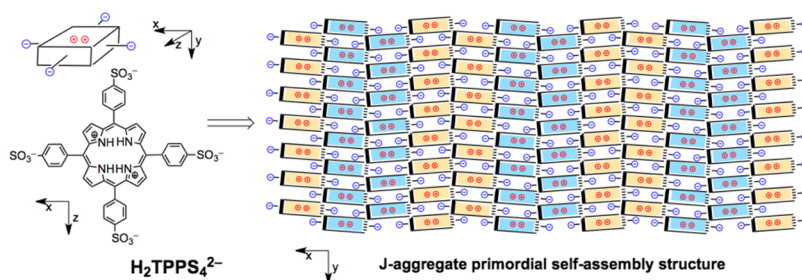


[a]The different colors of the porphyrin units, symbolized here as parallelepipedes, indicate two conformational enantiomers of the porphyrin monomer. This basic sheet structure evolves toward mono- or multilayers nanoparticles of different shapes.[7,11] Adapted with permission from ref 12.

**Scheme 2. Formula Scheme of Diprotonated *meso*-4-Sulfonatophenyl-substituted Porphyrins Discussed in This Work and on the Diastereoisomerism Arising from the Relative configuration of the Out-of-Plane 10- and 20-Meso Substituents of the J-Aggregate Primordial Sheet**
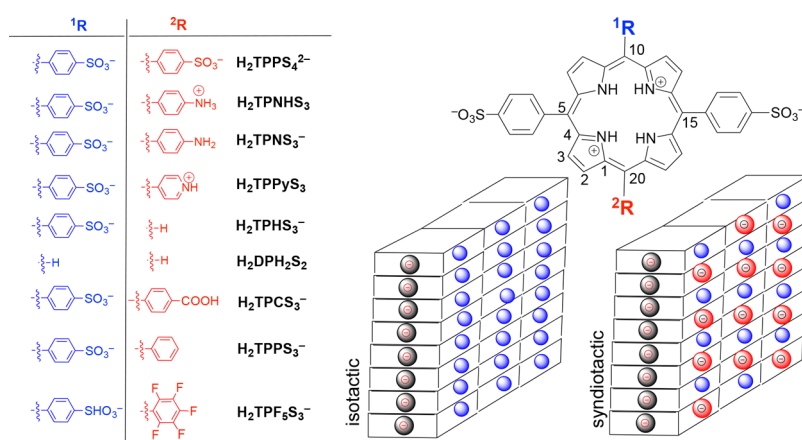


diastereoisomerism becomes possible because of the tacticity of substituents at both sheet sides (see Scheme 2).

In respect to (b), the sheet structure may evolve toward nanoparticles of different shapes, for example, single-walled nanotubes or plates of different morphologies composed by mono-, bi-, or multilayers of the fundamental structure. This evolution depends on the preparation method of the particles and on the peripheral substitution pattern of the monomeric diprotonated porphyrin. Curvature changes of the primary planar sheet obviously will occur according to its elasticity,[7] but note that the forces leading to the curvature effects belong to those originated by the diffuse electric-double layer (EDL) potentials of the surface, that is, to the topics relating EDL to the transition of micelles to spheres and cylinders and to the stability of charged membranes.[13−15]

Here, we present experimental evidence showing how the comparison between the $H_2TPPS_4^{2-}$ J-aggregate nanoparticles and those of other members of the homologous family (Scheme 2) gives a new insight on the origin of the stability of such a monomolecular-thick chiral sheet. The diastereomeric disorder generated by a structurally different meso-substituent group has not only influence on its stability but also on the structure and the topology of the particles upon further growth and evolution of the 2D-sheet monolayer.

### ■ RESULTS

Solutions of J-aggregates of the diprotonated porphyrins free of metallic cations were prepared according to previous reports

(Experimental Section). The presence of metallic counter-cations, for example, sodium ions, leads to the formation of inorganic salt crystallites which, besides the formation of nanoparticle clumps, hinder the use of scanning probe microscopy (SPM) methods.[7,16] For the preparation of the J-aggregate solutions, we used the Balaban method of capillary injection of a concentrated mother solution of the zwitterionic porphyrin into water.[7] In the case of diluted solutions, the acidity generated by the zwitterionic porphyrin is too low for the full diprotonation of the porphyrin monomers: this drawback was conveniently avoided using previously acidified water (HCl, pH ≈ 2 for the experiments described herein). Such an experimental procedure for $H_2TPPS_4^{2-}$ leads exclusively to single-walled nanotubes. This turned out to be also the best method to prepare long-shaped nanoparticles of the rest of J-aggregates of the series. In order to obtain particles of different morphologies, the simple careful dropping of aliquots of the porphyrin mother solution into either stirred or unstirred acidic water was the method of choice.

$H_2TPPS_4^{2-}$ J-aggregates were compared to those of *meso*-tris(4-sulfonatophenyl)porphyrins bearing as a fourth meso-substituent a neutral or a positively charged group (Scheme 2). As it can be inferred from many previous reports (e.g., refs[4,17−20]), the structure of the particle is not only determined by the electrostatic forces between sulfonato anions and the diprotonated porphyrin ring, which by themselves are isotropic, that is, of a nondirectional character, but by
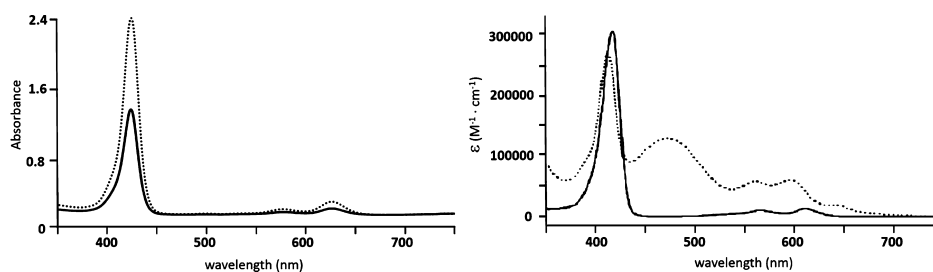
**Figure 1.** UV/vis absorption spectra of $H_2TPHS_3^-$ (4.5 $\mu$M and 0.8 mM) and $H_2DPH_2S_2$ (0.5 $\mu$M and 0.9 mM) J-aggregates UV/vis (mm cuvettes path length 1 cm and 0.01). At the $\mu$M concentration range (solid traces), no J-aggregates are formed. At the mM range (dotted traces), $H_2TPHS_3^-$ does not form J-aggregates, but $H_2DPH_2S_2$ yields J-aggregates of ill-defined geometry (broad absorption bands).
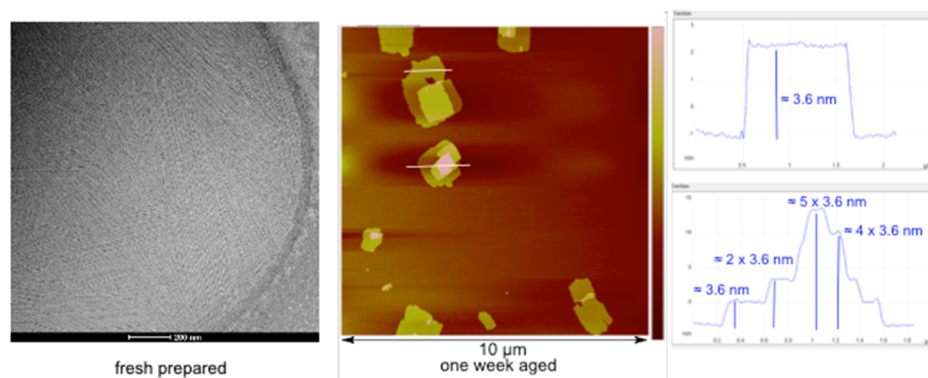


**Figure 2.** Cryo-TEM and SPM of $H_2TPCS_3^-$ J-aggregates (mica substrate). The first-formed single-walled nanotubes [peak force microscopy (PFM) on mica] evolve after few days toward large plates, which do not show enough contrast to be observed by CryoTEM, but can be observed by PFM.

hydrogen bonding, charge—dipole, dipole—dipole, and $\pi$ stacking which are of anisotropic character.

**Anionic Sulfonato Groups at Both Sides of the Sheet Surface.** $H_2TPPS_4^{2-}$: the aggregation of this porphyrin easily leads to single-walled nanotubes,[7,21,22] which show diameters in the range of $\approx$30 nm (see the Supporting Information). Bilayered nanoribbons are observed by SPM methods as a consequence of the nanotube collapse when the lumen squeezes when the solutions are casted on solid surfaces.[7] However, the preparation of the J-aggregate sample by a different method to that of the capillary injection described above can lead to bilayered nanoparticles whose dimensions, depending on the experimental procedure, are either too small or too large to achieve the required curvature of the nanotube cylinder.

The easy formation of nanotubes indicates a different behavior of the membranes composed of planar amphiphilic porphyrinic building blocks, showing multiple polar sites, to those of classical linear amphiphiles. Charged membranes of classical amphiphiles with identical ELDs at both membrane sides should be planar at the equilibrium.[13] It has been reported that charged micelles of linear amphiphiles evolve to vesicles placing the ionic charges at the convex side.[23] Note that in the case of $H_2TPPS_4^{2-}$ J-aggregates, both the convex and the concave side of the nanotubes show the same charge composition so that, on this basis, no deflection from planarity should be expected.

The curvature change from the planar sheet to a nanotube cylinder is determined by the free energy differences originated in the bending of the sheet. In this respect, the bending modulus along the $x$ and $y$ (see Scheme 1) axes must be different. Recent results using optical polarization spectroscopy

show that the circumference of the diameter section of the nanotube corresponds to the $x$ axis, that is, to the direction of J-aggregation.[24] Note that it is reasonable to expect higher free energy changes by the loss of the optimal geometry (curvature) of the $\pi$-stacking ($y$ axis) (H-aggregation exciton) than that along the J-aggregation exciton direction ($x$ axis).

**Anionic Sulfonato Groups and Noncharged Substituents at the Sheet Surface.** $H_2TPHPS_3^-$: acidic solutions of this porphyrin, even those at the mM range, show only the UV/vis absorption spectra of the diprotonated monomer (Figure 1). Partial formation of the J-aggregate could only be detected in solid films obtained by casting (Supporting Information). This negative result is significant in respect to discerning the origin of the effects that stabilize the J-aggregate sheet. In this respect, it is significant that the lack of aryl substituents at both sheet sides of the sheet (i.e., in the case of $H_2DPH_2S_2$) still allows the formation of J-aggregates, although without a defined geometry as indicated by the broad absorption bands of the UV/vis spectrum (Figure 1):[25,26] the absence of the effects generated by the peripheral aryl substituents at C10 and C20 reveals the isotropic, or of low directional character, of the electrostatic interaction between the diprotonated core and the anionic sulfonato groups. Furthermore, at high values of the ionic strength (0.3 M NaCl), the solutions of $H_2TPHS_3^-$ show a very weak but narrow J-aggregate absorption band (Supporting Information), pointing to a J-aggregate of low stability but with a well-defined geometry. This indicates that, in order for the J-aggregate to be stable, the forces originated at ELDs should be similar at both sides of the sheet, and that they do contribute significantly to obtain a specific geometry of the building blocks within the J-aggregate.

$H_2TPCS_3^-$: the carboxylate groups of this J-aggregate, because of the pH values necessary for their formation (monomer $pK_a = 4.7$), are present as neutral hydroxy carbonyl groups.

Freshly prepared solutions (capillary injection method) are exclusively composed by straight single-walled nanotubes (Figure 2): the lumen dimensions of the nanotubes of $H_2TPPS_4^{2-}$ and $H_2TPCS_3^-$ J-aggregates are of same order than those of $H_2TPPS_4^{2-}$. However, they evolve within a few days to wide plates mostly bilayered (i.e., composed of two 2D-sheets face-to-face to each other), although tri- and tetralayered terraces could be also observed (Figure 2). These slow changes of the morphology with time point to a kinetically controlled tacticity which leads to single-walled nanotubes at the initial stage of the aggregation process, which eventually self-repair to thermodynamically more stable morphologies.

With syndiotacticity or isotacticity being unlikely to emerge in a kinetically controlled formation of the J-aggregate, a reasonable assumption is a first formation of nanotubes with atactic surfaces, that is, statistically similar sheet surfaces, which evolve by ripening to larger areas of the J-aggregates (Ostwald-like ripening), so that they can achieve morphologies of higher stabilities. This ripening would break the nanotube structure. The ability of the hydroxycarbonyl groups for hydrogen bonding suggests that the isotactic configuration would favorably lead to the formation of larger-scale structures in which hydrogen bond interactions between the hydroxycarbonyl groups of two adjacent layers, and perhaps also between hydroxycarbonyl and sulfonato groups, allow the formation of multilayered particles (Scheme 3). Domains showing iso-tacticity or syndiotacticity would evolve to the formation of bilayers and multilayers.

$H_2TPPS_3^-$: the capillary injection method yields straight short single-walled nanotubes showing wall defects. Cryo-TEM imaging shows nanotubes with voids at their walls, even with

**Scheme 3. Scheme Showing How Isotacticity in $H_2TPCS_3^-$ J-Aggregates Yields the Adequate Geometry for the Formation of a Polymeric Hydrogen Bonding Interface between Two Sheets[a]**
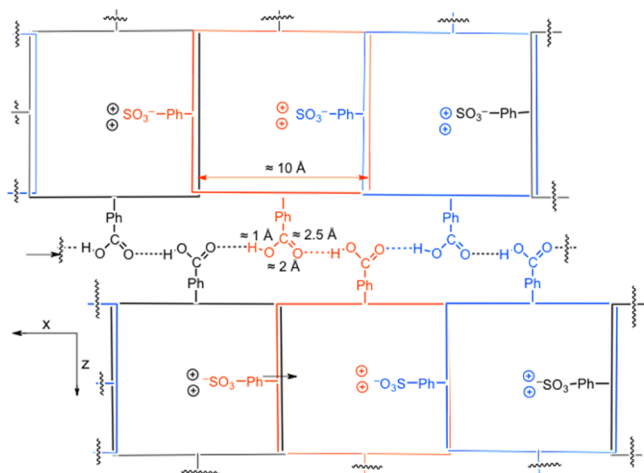


[a]Eventually, anionic sulfonato groups (partial isotacticity) acting as hydrogen bond acceptors could replace some carboxylic acid groups. Different tacticity domains would explain the ability to form plates composed of more than two sheets (Figure 2)

topological changes on the cylinder curvature (Figure 3). PFM imaging recognizes these defects when the nanotube collapsing to bilayered ribbons in deposition on dry HOPG or mica (Figure 3) is taken into account.

Samples prepared by dropping an aliquot of the porphyrin mother solution to the HCl solution yield irregular nanotubes. Cryo-TEM shows, in contrast with the nanotubes of the $H_2TPPS_4^{2-}$ and $H_2TPCS_3^-$ J-aggregates, nonstraight nanotubes, some of them of nonconstant diameter, voids in their walls, and even forming ramified structures (Figure 4). These nanotubes, when deposited onto the solid substrates for SPM imaging, collapse to the bizarre bilayered helical ribbons that have been previously reported (e.g., ref 27). Although incomplete formation of nanotubes has been reported,[4] their topology is different to the bizarre structures that may be obtained in the case of $H_2TPPS^{3-}$. Nanoparticles, either too wide or too small to form nanotubes, were always detected as bilayers, but never forming multilayered structures. However, when the SPM imaging was immediately performed after the sample preparation, some few monolayered particles could be detected, which then disappear after a short time. All these point to the self-repairing to the isotactic configuration driven by the formation of an interface between two monolayers.

$H_2TPF_5S_3^{3-}$: only monolayered particles were detected for this J-aggregate. However, as previously reported,[28] different nanoparticles can show slight differences in their thickness (1.80–2.45 nm) depending on the preparation method. Such a difference of thickness again points to different tacticities. The lack of bilayered particles, in contrast with $H_2TPPS_3^-$ J-aggregates, may be attributed to a lower water exclusion effect of the pentafluorophenyl groups than that of the phenyl ones. Note that the interaction between the pentafluorophenyl substituents of two monolayers cannot be, by sterical reasons, the optimal $\pi$-stacking for the pentafluorophenyl substituents because it corresponds to an overlapping between two $F-C^{sp^2}$ groups or between one $F-C^{sp^2}$ group and the pentafluorophenyl ring. However, in the case of $H_2TPPS_3^-$ J-aggregates, the interlayer interaction between lateral phenyl substituents is between the $H-C^{sp^2}$ group and the phenyl substituent. Such an interpenetration between lateral groups at the interface should result in a higher water exclusion effect for $H_2TPPS_3^-$ than for $H_2TPF_5S_3^-$.

The capillary injection method allows the preparation of wide plates, which when observed by cryo-TEM show the expected sheet structure (Figure 5). The sheets show small curvatures from planarity but a shape change from convex to concave at the middle of their surface. Note that the principal contribution to the visualization by CryoTEM of the J-aggregate nanoparticles is that of the electron scattering of their sulfur atoms, which are the heaviest of their chemical composition.[7] Furthermore, in the case of nanotubes, electron scattering effects enhance the contrast. Even electron diffraction structural evaluations have been reported.[29] The observation of simple sheets in the case of $H_2TPF_5S_3^-$ must be attributed to the substitution of some H atoms by F atoms.

**Anionic Sulfonato Groups and Cationic Substituents at the Sheet Surface.** A characteristic of the family of 4-sulfonatophenyl-substituted porphyrin J-aggregates is the detection of CD signals because of the presence of small biases from the racemic composition (see, e.g., ref 25). Such racemic biases are the signature of a spontaneous mirror symmetry breaking (SMSB) of the self-assembly process as a
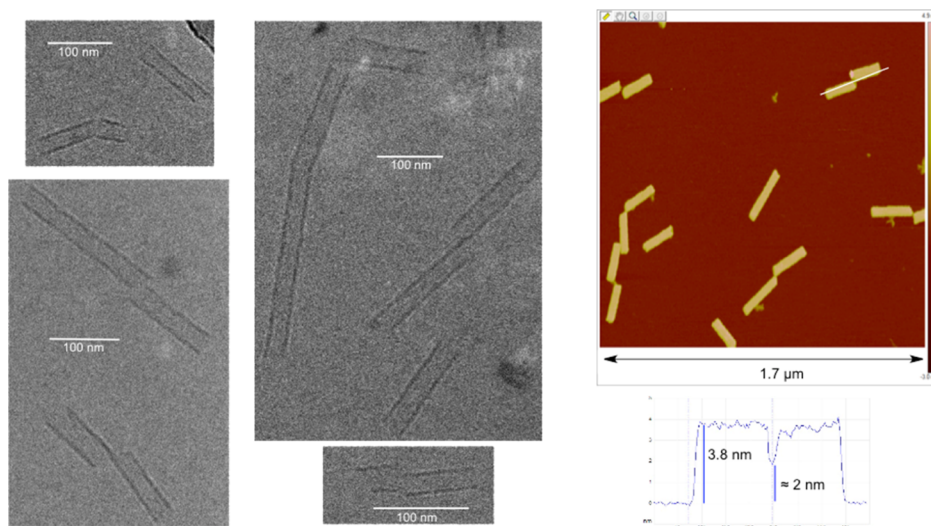
**Figure 3.** CryoTEM and PFM imaging of $H_2TPPS_3^-$ J-aggregate nanotubes obtained by the capillary injection of the mother porphyrin solution into a stirred acidic solution. In contrast with the J-aggregate nanotubes of other porphyrins, their walls show voids and defects from linear growth and even the change of the curvature.
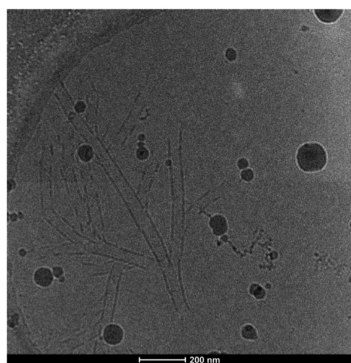


**Figure 4.** CryoTEM imaging of $H_2TPPS_3^-$ J-aggregate nanotubes obtained by dropping a porphyrin mother solution into the acidic HCl solution (the black drops correspond to the initial phase of the transformation of vitrified water to crystallized water). The defects observed in the case of the capillary injection preparation method (Figure 3) are now enhanced yielding arborescent structures of irregular single-walled nanotubes. By SPM these samples show, after their deposition on dry substrates, a collapse (ref 7) to the characteristic helical bundles of ribbons previously reported (e.g., ref 27).
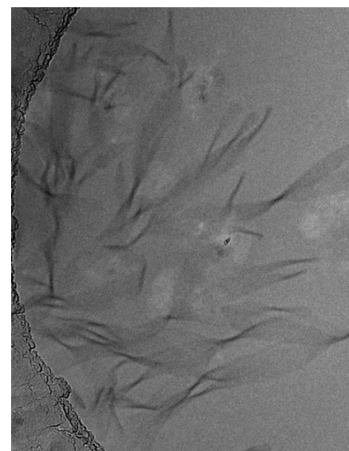


**Figure 5.** CryoTEM images of monolayer sheets of $H_2TPF_5S_3^-$ J-aggregates. Their thickness, measured by PFM, agrees with monolayers of slightly different thickness as expected for different tacticities.

whole at the bifurcation from achiral building blocks to a scalemic mixture of chiral supramolecular structures: SMSB processes are extremely sensitive to chiral polarizations and dramatic experimental examples of this sensitivity have been reported.[30−33] Notice that any first enantiomeric excess, obtained at the primary "nucleation" stage, such as the one occurring in crystallization,[34] is simply transferred, but not amplified, during the growth stage. However, in the direct preparation of $H_2TPPNHS_3$ and $H_2TPPyS_3$ J-aggregates, no CD signals could be detected in any case. This absence of CD signals can be attributed either to the formation of a real racemic composition of chiral supramolecular structures or because the secondary structure of these two J-aggregates is itself achiral. Notice that the sheet structure could belong to a monoclinic space group of higher symmetry, that is, achiral, than that of $P2_1$.

$H_2TPNS_3^-$ and $H_2TPNHS_3$: these J-aggregates are interconverted by changing the solution pH value and their interconversion can be followed by the changes of the absorption spectra, as well by their nanoparticle morphology.[35] This can be observed because of the lower $pK_a$ values of the aminophenyl derivative ($pK_a$ = 2.8) in respect to the diprotonation of the porphyrin ring ($pK_a$ = 5.1). In the case of $H_2TPNS_3^-$, the nanoparticle morphology observed by PFM is in accordance with bilayered folded irregular ribbons; however, cryoTEM was not able to distinguish whether or not they have a nanotube morphology in the solution pH values leading to the ammonium derivative $H_2TPNHS_3$ generate a J-aggregate with flocculation-like crystallite particles. This behavior suggests a strong ionic interaction between different sheets of the peripheral anionic sulfonato groups and the cationic ammonium ones.

$H_2TPPyS_3$: this porphyrin shows the protonation of the pyridine substituent to a pyridinium cation ($pK_a$ = 5.4) before the diprotonation of the porphyrin ring takes place ($pK_a$ = 3.9). Therefore, $H_2TPPyS_3$ J-aggregates always bear the

positively charged pyridinium group. It is surely significant that the absorption spectra of $H_2TPPyS_3$ J-aggregates show absorption peaks, manifested as shoulders (460−480 nm: see Figure 6), below the limit of the red shift of the maximal coherent length of the J-excitonic band. This points to the presence of shorter sheet lengths along the $x$ axis.[16]
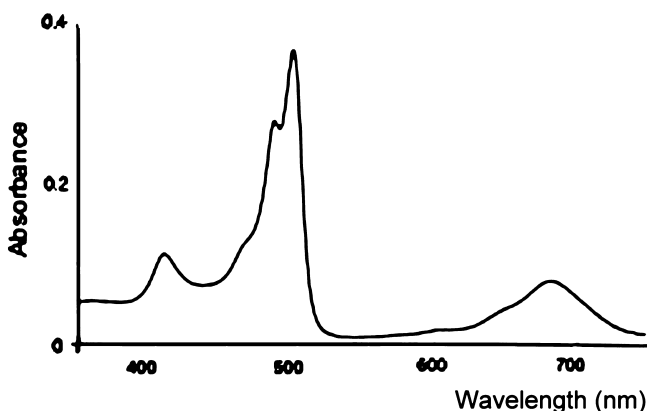


**Figure 6.** UV/vis absorption spectra of $H_2TPPyS_3$ (≈1 mM: cuvette path length = 0.01 mm) J-aggregates showing strongly shifted H- and J-aggregate excitonic bands (410 and 501 nm respectively compared to the B-band of the diprotonated monomer 437). The presence of bands with lower red shifts (shoulders at 467 and 488 nm) indicates the presence of shorter sheets along the $x$ axis (see Scheme 1).

Despite the fact that morphologies such as those of the $H_2TPNHS_3$ J-aggregates could be expected, the nanoparticle morphology for $H_2TPPyS_3$ J-aggregates is that of bilayered plates (≈3.9 nm). However, some of the nanoparticles show thicknesses that agree with the deposition of monomeric porphyrin units on the top of the bilayer (≈3.9 + 0.9 nm: see Figure 7). This deposition, as well as the formation of the
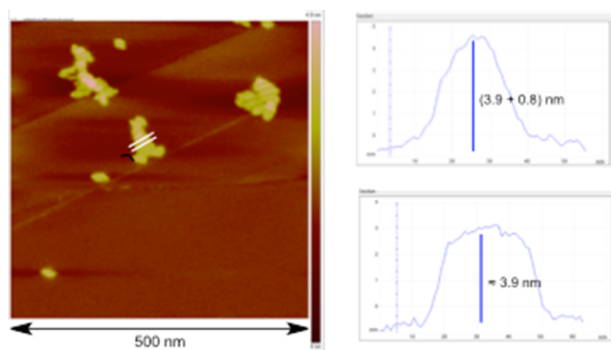


**Figure 7.** PFM image of $H_2TPPyS_3$ aggregates (HOPG). The relatively small nanoplates are all bilayered, but some of them show that monomeric porphyrin deposit on the top of the plate.

bilayers, is originated by the electrostatic interaction between the cationic pyridinium groups and anionic sulfonates at the sheet surface. Such deposition is clearly different to the commonly observed when a monomer deposites on the graphite surface (HOPG): the diprotonated monomer mostly present in some proporting in J-aggregate solutions, deposites planar (thickness ≈ 0.8−0.9 nm) upon HOPG. It is also different to the deposition of small J-aggregate particles on the top of bigger ones as observed in the case of mica substrates,[7]

that in our opinion may lead to misunderstandings on the discussion of SPM results.

## ■ DISCUSSION

The fundamental structure of these nanoparticles arising from the self-assembly is a 2D crystal that shows a low exchange rate of unitary building blocks with the solution. This exchange rate is similar to that of a crystal in its saturated solution, where exchange takes place at the crystal surface. However, in such a 2D crystal-like structure, the building block exchange would occur at the edges of the structure, that is, at the $x$ or $y$ axes (see Scheme 1) boundary of the sheet with the solution, but not along the $z$ axis. In this respect, it is worth noting that a recent report relates the lack of relaxation rates of the primordial self-assembly structures with the increase in freedom degrees forming diverse nanoparticle morphologies.[8,36]

Despite the absence of the degree of stability of the J-aggregate sheet structure that would imply a further progression to a 3D crystal-like structure of the nanoparticle along the $z$ axis, strikingly, the two-dimensional monolayer still shows a well-defined crystal ordering (space group $P2_1$)[12] The comparison of the effect that different meso-substituents have at the sheet surfaces shows how the role that 3D growth has in the stabilization of crystals in these J-aggregate 2D crystals is replaced by the forces originated by solvent and counter ions at the EDLs at both sheet surfaces. These forces act as building fundaments supporting the sheet. Two identical strong EDLs contribute to the stability of the J-aggregate monolayer in the solution. In this respect, the behavior of $H_2TPPS_4^{2-}$ with those of $H_2TPHS_3^-$ and $H_2DPH_2S_2$ is compared. $H_2TPPS_4^{2-}$ and $H_2DPH_2S_2$ show identical forces at both sheet surfaces, but in the case of $H_2DPPS_2$ the forces, being lower to those of its counterpart, cannot fix the sheet structure to a specific geometry as it is the case of the rest of tested porphyrins.

The formation of a water layer near the surface appears also as a consequence of the EDL potential. Such a water layer is also formed on surfaces without charged substituents. However, the results show that the effect of such a water layer is less significant when the meso position is unsubstituted ($H_2TPHS_3^-$) than when it is occupied by a hydrophobic phenyl group ($H_2TPPS_3^-$). Similar forces originated by ion and water movements at both sides of the sheet, despite being the result of different types of EDL potentials (negative, positive, or neutral surfaces) may also stabilize the sheet. For the tested porphyrins different to $H_2TPPS_4^{2-}$, atactic relative configurations lead to statistically configured domains of similar EDL potentials at both side surfaces. However, in the case of $H_2TPHS_3^-$, the quite different electronic and steric characteristics of a H atom compared to a 4-sulfonatophenyl group does not drive the system toward aggregation: only with the presence of sodium and chloride counterions, which generate higher forces, it is possible to detect a low concentration of J-aggregates showing a defined geometry (see the Supporting Information) in contrast to $H_2DPH_2S_2$.

The formation of irregular nanotubes $H_2TPPS_3^-$ with wall defects reveals how the possibility to have different tacticities does not favor the nanotube formation. Note that the nanotube diameter (20−30 nm) determines a lumen radii much larger than the electrostatic double layer screening-length and that this implies the presence of lumen bulk water that will free exchange with the water solution through the open ends of the nanotube. The change from atacticity to

isotacticity would lead to different potentials inside and outside of the nanotube and the results obtained with $H_2TPCS_3^-$ would agree with this: only atacticity (freshly prepared J-aggregates) leads to nanotubes.

In the nanotubes, the radii of curvature of the surfaces are large compared to the electrostatic screening length. This suggests that the nanotube formation may occur when the free energy differences originated by the concave and convex curvatures are of a contrary sign. Probably significant curvatures occur when both surfaces show very similar EDPs: identical for $H_2TPPS_4^{2-}$ and, for example, statistically similar for atactic $H_2TPCS_3^-$. $H_2TPF_5S_3^-$ shows a tendency to build different tacticity domains as inferred from the detection of monolayers of different thicknesses.[28] This would not favor the appropriate curvature leading to the formation of nanotubes.

In the case that isotactic domains may lead to interactions between surfaces, bilayered nanoparticles would arise by forming additional interactions at the newly rearranged interface ($H_2TPCS_3^-$) or water exclusion effects ($H_2TPPS_3^-$). For positively and negatively charged surfaces, ($H_2TPNHS_3$ and $H_2TPPyS_3$), the results suggest a role for electrostatic interactions between oppositely charged isotactic or syndiotactic domains in the formation of bilayers. In summary, the formation of bilayers in the solution takes place if there is a free energy gain thanks to the formation of an interface, for example, by hydrogen bonding ($H_2TPPCS_3^-$), water exclusion effects ($H_2TPPS_3^-$), or electrostatic favorable interactions ($H_2TPNHS_3$ and $H_2TPPyS_3$).

Chemical reasoning suggests that the sheet may act as a permeable membrane for proton exchange. This would occur between the surfaces composed of solvated protons at the diffuse monolayer through the NH sites of the porphyrin ring. Such a proton-transfer mechanism, the so-called of Grotthuss's mechanism,[37] is faster than the diffusion of any other species and of about the same order than the vibrational rates. Therefore, the sheet geometry would not relax under an exchange this fast. Note that for bilayered systems with a hydrophobic interface, this fast permeability to proton exchange would not be possible.

In respect to the chiral structure of the J-aggregate, the role of the EDPs suggests that the twists of the porphyrin building blocks along the axis $x$ and $y$ arise because of the forces acting at both sides of the sheet which cause the transition from metastable achiral structures to two enantiomorphs. In addition, the formation of these J-aggregates is a process showing autocatalytic growth (cooperative primary self-assembly similar to primary nucleation in crystallization),[11] that is, both necessary conditions for SMSB are met.[38] Previous reports on the dramatic effects of hydrodynamic shear forces in the deterministic selection of their chiral sign[30,32,33] had confirmed this. Note how the present results strongly suggest that fluctuations of the hydrodynamic forces originate by the electrical double layer determining the transition from achiral metastable sheets to stable chiral ones. This means that each nanoparticle sheet undergoes SMSB and, in the absence of any chiral polarization at the bifurcation point, there is a stochastic distribution of chiral signs, that is, a racemic mixture of J-aggregate sheets is obtained. However, owing to the dynamics of their growth, and in the presence of an effective, however weak, chiral polarization at the bifurcation point, a bias from the racemic composition can be amplified to the detectable levels.

Therefore, chiral shear forces at this bifurcation point would determine the selection of the chiral sign, such as that which has been experimentally observed.[30,32,33]

The comparison of the tertiary structures of these different J-aggregates suggests that in respect to potential applications,[39,40] for example, in their use as energy and proton-transfer devices, the J-aggregates of choice are the nanotubes obtained from $H_2TPPS_4^{2-}$.

## ■ EXPERIMENTAL SECTION

**Methods.** p$K_a$ values of the monomeric water-soluble porphyrins were spectrophotometrically measured at room temperature by monitoring the absorbance changes at a fixed wavelength (typically at an absorption maximum of one of the species involved in the acid–base equilibrium) in micromolar solutions of the substance at different pH values. The p$K_a$ values were then determined using the Henderson–Hasselbalch equation.[41] All the spectra used in the p$K_a$ determinations showed adequate isosbestic points.

CD measurements of J-aggregate samples were performed according to the methods previously described in order to exclude artifactual CD signals (see, e.g., ref 20 and citations therein).

SPM methods were routinely applied for topological assignment of mono- and bilayered structures. For section analysis of the nanoparticles, peak force microcopy was used preferentially to atomic force microscopy: for instrument and experimental details, see ref 7 and citations herein.

*Peak Force Microscopy.* Images were acquired on a multimode atomic force microscope attached to a Bruker Nanoscope V electronics unit. For these experiments, the scan-assist tapping mode was used. For more experimental details, see ref 7 and cites therein. The solution deposition procedure for PFM imaging on dry substrates: one drop (10 mL) of the nanoparticle solution was brought into contact with a freshly cleaved HOPG or mica surface for a specific time interval and the solution was then blotted off with the tip of a sheet of filter paper. Finally, the substrate surface was dried by blowing with a stream of $N_2$.

*Cryo-TEM.* The J-aggregate $H_2TPPS^{3-}$ solutions were visualized by the cryo-TEM method. A thin aqueous film was formed from the suspension by dipping and withdrawing a bare specimen grid. Glow-discharged holey carbon grids were used. After withdrawal from the suspension, the grid was blotted against the filter paper, leaving thin sample films spanning the grid holes. These films were vitrified by plunging the grid into ethane, which was kept at its melting point by liquid nitrogen, by using a Vitrobot (FEI Company, Eindhoven, the Netherlands), and keeping the sample before freezing at 100% humidity. Vitrification of the thin films was initiated at room temperature. The vitreous sample films were transferred to a Tecnai F20 microscope (FEI Company, Eindhoven, Netherlands) by using a Gatan cryotransfer. The images were taken at 200 kV between −170 and −175 °C and by using low-dose imaging conditions.

**Preparation of the Zwitterionic Forms (Absence of Metallic Counter Cations).** Solutions of concentrated diprotonated zwitterionic porphyrins for sample preparation of HJ-aggregates were prepared by passing a solution of about 3 mg of lyophilized porphyrin in 1 mL pure water through a Dowez 50WX4: 200/400 mesh (acid form) cationic exchange column (acid form). The eluted solution (2 mL) were used as concentrated mother solutions ($1 \times 10^{-3}$ to $1 \times 10^{-4}$ M).

*Preparation of J-Aggregate Samples.* Samples for the preparation of nanotubes were prepared by capillary needle injection of the zwitterionic mother solution (250 μL) in a HCl pH = 2 acid solution; for more experimental details, see ref 7; in order to obtain nanoparticles of different shapes also, the simple drop to drop addition of 250 μL to the acidic water solution either by stirring or waiting for spontaneous diffusion of the solutions was used.

5-(4-Pyridyl)-10,15,20-tris(4-sulphonatophenyl)porphyrin (TPPyS$_3$$^{3-}$) was obtained by sulfonation of 5,10,15-triphenyl-20-(4-pyridyl)-porphyrin (PyTPP),[42] according to the following procedure: in a 10 mL round-bottomed flask at 0 °C, 250 mg of PyTPP was dissolved in 4 mL of conc. H$_2$SO$_4$ under sonication and magnetic stirring. An intense greenish homogeneous solution was obtained, which was heated up to 105 °C and stirred over 6 h. It was then left to cool under stirring overnight. The mixture was added to cold water (50 mL) to stop the reaction, and the resulting solution was centrifuged once it was at room temperature. While the supernatant liquid was rejected because of its content of undesired sulfuric acid and salts, the greenish crude obtained (precipitate) was dissolved in a few mL of water and then neutralized with a Na$_2$CO$_3$ saturated solution until the greenish color turned reddish. The crude was purified by reversed-phase chromatography (eluted with H$_2$O/CH$_3$OH 1:1), and the purest salt-free fractions were lyophilized: sample compositions were monitored by HPLC. Yield: 278 mg (74%) of purple crystals. The p$K_a$ value for porphyrin ring diprotonation is 3.9.

$^1$H NMR (DMSO-$d_6$, 400 MHz): δ (ppm) 9.02 (d, 2H, 3,5-pyridyl), 8.85 (m, 8H, β-pyrrol), 8.27 (d, 2H, 2,6-pyridyl), 8.17 (d, 6H, 2,6-phenyl), 8.03 (d, 6H, 3,5-phenyl), 2.07 (s, NH), −2,97 (s, 2H, NH-pyrrol).

ESI−MS (negative mode): C$_{43}$H$_{26}$N$_5$O$_9$S$_3$: *m/z* calcd for [M]$^{3-}$, 284.03; found, 284.03. *m/z* calcd for [C$_{43}$H$_{27}$N$_5$O$_9$S$_3$]$^{2-}$, 426.55; found, 426.55.

5,10,15-Triphenylporphyrin: In a 1 L round-bottomed flask with agitation, EtOH (500 mL) was placed and argon was bubbled in the solution for 15 min. Dipyrromethane (0.5 g, 3.5 mmol),[43] 5-phenyldipyrromethane[44] (0.78 g, 3.5 mmol), and benzaldehyde (0.7 mL, 7 mmol) were added. The reaction mixture was stirred for 10 min under argon and 133 mL of HCl (0.27 mM) was added. The flask, shielded from light, was stirred at room temperature for 16 h under argon. The reaction crude was extracted with CH$_2$Cl$_2$ (200 mL) and the organic phase was washed with a saturated aqueous solution of Na$_2$CO$_3$ (200 mL), then with water (200 mL), and dried on anhydrous MgSO$_4$. *p*-Chloranil (340 mg, 1.38 mmol) was added to this organic phase that was heating to reflux for 1 h. The final product was purified by crystallization in acetonitrile (20 min heating at reflux). The liquid solution was separated from the precipitate and rotary evaporated. Purification by preparative TLC (*n*-hexane/ethyl acetate, 15:1) yields 46 mg (3%) of a violet solid.

$^1$H NMR (CDCl$_3$, 400 MHz): δ (ppm): 10.23 (s, 1H, H−C20), 9.35 (d, *J* = 4.5 Hz, 2H, H3), 9.03 (d, *J* = 4.5 Hz, 2H, H−C2 and H−C18), 8.89 (m, 4H, H−C7, H−C8, H−C12 and H−C13), 8.25 (m, 6H, ortho-H), 7.79 (m, 9H, meta- and para-H), −3.00 (s, 2H, H−N).

ESI−MS (positive mode): C$_{38}$H$_{26}$N$_4$: *m/z* calcd for [M + H]$^+$, 539.2; found, 539.3.

5,10,15-Tris(4-sulfonatophenyl)porphyrin (TPHPS$_3$$^{3-}$): Sufonation of 5,10,15-triphenylporphyrin is as follows. The

starting porphyrin (7 mg, 0.013 mmol) was transferred on a small round-bottomed flask. Then, 2 mL of H$_2$SO$_4$ (98%) was added. The reaction mixture was stirred for 4 h at 80 °C. After 4 h, 1 mL of water was added to the reaction media and the solution was neutralized with saturated NaHCO$_3$ solution (≈80 mL). The final solution was purified through a reverse-phase C18 column: inorganic salts were separated by water elution and the elution with MeOH/H$_2$O (1:1) allowed the separation of reaction subproducts. The eluted fraction compositions were analyzed by HPLC: red solid; 3 mg, 30% yield.

$^1$H NMR (CD$_3$OD, 400 MHz): δ (ppm) 10.43 (s, 1H, H−C20), 9.51 (d, *J* = 4 Hz, 2H, H−C2, and C18), 9.02 (d, *J* = 4 Hz, 2H, H−C3, and C17), 8.92 (m, 4H, H−C7, H−C8, H−C12, and H−C13), 8.31 (m, 12H, ortho-, and meta-H).

ESI−MS (negative mode): C$_{38}$H$_{23}$N$_4$O$_9$S$_3$: *m/z* calcd for [M]$^{3-}$, 258.3; found, 258.5.

5-(4-Hydroxycarbonylphenyl)-10,15,20-triphenylporphyrin: to freshly distilled CH$_2$Cl$_2$ (1 L) in a three-neck round-bottomed flask (2 L), pure N$_2$ was bubbled for 15 min under stirring. Then, under stirring and under N$_2$ atmosphere, 1.910 g (18 mmol) of benzaldehyde, 984 mg (6 mmol) of methyl 4-formylbenzoate, and 1.612 g (24 mmol) of pyrrole were added. After that, 0.25 mL (2 mmol) of BF$_3$ in ether solution was added. The flask was protected from direct light and kept under nitrogen atmosphere. Some minutes after the BF$_3$ addition, the reaction mixture changed from colorless to orange; 15 min later, the dark solution was further stirred (2 h). Then, 3.7 g (15 mmol) of *p*-chloranil was added and the reaction was left stirring for another 20 h. The solution was evaporated under reduced pressure to a final volume of 200 mL. Vacuum filtration through silica removes linear pyrrole pigments and other polar components. The final reaction crude was purified by flash chromatography (CH$_2$Cl$_2$/hexane (3:2) and dry loading). TLC of the crude showed the presence of many spots, later identified as TPP, TPC, TPC$_2$O, and TPC$_2$A. TPPC was dissolved in MeOH (HPLC quality), neutralized with Na$_2$CO$_3$, and filtered. The solution was then evaporated under reduced pressure and recrystallized dissolved in the minimum amount of MeOH (HPLC quality) at 80 °C. The crystalline solid was separated and dried over P$_2$O$_5$ to yield a purple solid: 550 mg (0.835 mmol), 14% yield.

UV/vis (CH$_2$Cl$_2$): 5.9 × 10$^{-6}$ M; λ, nm (ε): 418 (330 000), 515 (14 900), 550 (7200), 589 (5400), 645 (4100.).

$^1$H NMR (400 MHz, CDCl$_3$): δ (ppm) 8.8 (m, 8H, H−C$_{Pyrr}$), 8.4 (d, 2H, H−Ar), 8.3 (d, 2H, H−Ar), 8.2 (m, 6H, H−Ar), 7.8 (m, 9H, H−Ar), 4.1 (s, 3H, CH$_3$OCO−Ar).

MS (MALDI-TOF): C$_{46}$H$_{32}$N$_4$O$_2$: *m/z* calcd for [M]$^+$, 674.26; found [M]$^+$, 672.30; *m/z* calcd for [M + 1]$^+$, 673.26; found, 673.30.

TLC (CH$_2$Cl$_2$/hexane 4:1, $R_f$ 0.55) showed a single spot with a tail because of ester hydrolysis (observed by bidimensional TLC) that is not an issue for the following sulfonation purposes.

5-(4-Hydroxycarbonylphenyl)-10,15,20-tris(4-sulfonatophenyl)-porphyrin (TPCS$_3$$^{3-}$). Sulfuric acid (50 mL, 98%) was slowly added to 550 mg of 5-(4-hydroxycarbonylphenyl)-10,15,20-triphenylporphyrin in a 100 mL round-bottomed flask equipped with a Dimroth condenser. The reaction mixture was heated to 100 °C and stirred. After 24 h, 10 mL of ice/water was added to the reaction mixture. The solution was centrifuged and the supernatant separated and recentrifuged. The porphyrin precipitates were collected together and

neutralized to pH 7 with a saturated solution of Na$_2$CO$_3$. Extractions with CH$_2$Cl$_2$ eliminated traces of unsulfonated porphyrin. The aqueous solution containing inorganic salts and sulfonated porphyrins was evaporated under reduced pressure. The resulting crude was refluxed with MeOH, filtrated, and then rotatory evaporated. The final evaporation residue was eluted through a reverse-phase C18 column using MeOH/water (50:50) as a starting eluent, and decreasing polarity until MeOH 100%. The purity of the porphyrin fractions was monitored by HPLC: reaction byproducts were detected before (unknown compound) and after (meta-sulfonated product) the TPCS$_3^{3-}$ peak. This procedure proved to be ineffective in order to fully separate TPPS3C from the metasulfonated derivative. However, the MCI GEL CHP20P column using water as eluent was effective when the TPPS3C crude contained small amounts of polar and metasulfonated byproducts: the TPCS$_3^{3-}$ was retained into the column under water elution, it was eluted with MeOH/water (1:4), and the meta-sulfonated derivative was extracted from the column with MeOH 100%. The salt-free TPCS$_3^{3-}$ (purity 95%) was lyophilized yielding 50 mg (5.07 × 10$^{-2}$ mmol), yield 6%, of Na$_4$TPPS$_3$C 95%.

UV/vis (water): 1.8 × 10$^{-6}$ M; λ, nm (ε): 414 (480 000), 516 (15 900), 553 (7000), 581 (6000), 634 (4000). The p$K_a$ value for porphyrin ring diprotonation is 4.7.

$^1$H NMR (400 MHz, DMSO-$d_6$): δ (ppm) 8.83 (m, 8H, H–C$_{pyrr}$), 8.26, 8.16. 8.09, 8.02 (4d, 8H, J ≈ 8 Hz, A$_2$B$_2$ system of the ortho and meta H–C$_{Ar}$).

MS (ESI, negative mode): C$_{45}$H$_{26}$N$_4$O$_{11}$S$_3$: m/z calcd for [M + H]$^{3-}$, 298.3565; found, 298.3650; m/z calcd [M + 2H]$^{2-}$, 448.486587; found, 448.5457.

## ASSOCIATED CONTENT

**Supporting Information**

The Supporting Information is available free of charge on the ACS Publications website at DOI: 10.1021/acsomega.8b03176.

Experimental details; porphyrin monomer synthesis; additional UV/vis and NMR spectra; cryo-TEM images of H$_2$TPPS$_4^{2-}$ J-aggregate nanotubes; UV/Vis absorption spectra of H2TPHS3; absorption spectra of the solid film obtained by evaporation on a quartz plate of an acidconcentrated solution of H$_2$TPHPS$_3^-$ showing the partial formation of J-aggregate; and comparison of the UV/Vis absorption spectra of fresh (dotted line) and aged solutions (boldline) of the H$_2$TPCS$_3^-$ J-aggregates (PDF)

## AUTHOR INFORMATION

**Corresponding Author**
*E-mail: zelhachemi@ub.edu (Z.E.-H.).

**ORCID**
Zoubir El-Hachemi: 0000-0003-0537-5541

**Notes**
The authors declare no competing financial interest.

## REFERENCES

(1) Elemans, J. A. A. W.; van Hameren, R.; Nolte, R. J. M.; Rowan, A. E. Molecular Materials by Self-Assembly of Porphyrins, Phthalocyanines, and Perylenes. Adv. Mater. 2006, 18, 1251−1266.
(2) D'Souza, F.; Smith, P. M.; Zandler, M. E.; McCarty, A. L.; Itou, M.; Araki, Y.; Ito, O. Energy Transfer Followed by Electron Transfer in a Supramolecular Triad Composed of Boron Dipyrrin, Zinc Porphyrin, and Fullerene: A Model for the Photosynthetic Antenna-Reaction Center Complex. J. Am. Chem. Soc. 2004, 126, 7898−7907.
(3) Winters, M. U.; Dahlstedt, E.; Blades, H. E.; Wilson, C. J.; Frampton, M. J.; Anderson, H. L.; Albinsson, B. Probing the Efficiency of Electron Transfer through Porphyrin-Based Molecular Wires. J. Am. Chem. Soc. 2007, 129, 4291−4297.
(4) Rich, C. C.; McHale, J. L. Influence of Hydrogen Bonding on Excitonic Coupling and Hierarchal Structure of a Light-Harvesting Porphyrin Aggregate. Phys. Chem. Chem. Phys. 2012, 14, 2362−2374.
(5) Fukui, T.; Kawai, S.; Fujinuma, S.; Matsushita, Y.; Yasuda, T.; Sakurai, T.; Seki, S.; Takeuchi, M.; Sugiyasu, K. Control over Differentiation of a Metastable Supramolecular Assembly in One and Two Dimensions. Nat. Chem. 2016, 9, 493−499.
(6) Venkata Rao, K.; Miyajima, D.; Nihonyanagi, A.; Aida, T. Thermally bisignate supramolecular polymerization. Nat. Chem. 2017, 9, 1133−1139.
(7) El-Hachemi, Z.; Balaban, T. S.; Campos, J. L.; Cespedes, S.; Crusats, J.; Escudero, C.; Kamma-Lorger, C. S.; Llorens, J.; Malfois, M.; Mitchell, G. R.; Tojeira, A. P.; Ribó, J. M. Effect of Hydrodynamic Forces on meso-(4-Sulfonatophenyl)-Substituted Porphyrin J-Aggregate Nanoparticles: Elasticity, Plasticity and Breaking. Chem.—Eur. J. 2016, 22, 9740−9749.
(8) Mabesoone, M. F. J.; Markvoort, A. J.; Banno, M.; Yamaguchi, T.; Helmich, F.; Naito, Y.; Yashima, E.; Palmans, A. R. A.; Meijer, E. W. Competing Interactions in Hierarchical Porphyrin Self-Assembly Introduce Robustness in Pathway Complexity. J. Am. Chem. Soc. 2018, 140, 7810−7819.
(9) De Napoli, M.; Nardis, S.; Paolesse, R.; Vicente, M. G. H.; Lauceri, R.; Purrello, R. Hierarchical Porphyrin Self-Assembly in Aqueous Solution. J. Am. Chem. Soc. 2004, 126, 5934−5935.
(10) Gaeta, M.; Raciti, D.; Randazzo, R.; Gangemi, C. M. A.; Raudino, A.; D'Urso, A.; Fragalà, M. E.; Purrello, R. Chirality Enhancement of Porphyrin Supramolecular Assembly Driven by a Template Preorganization Effect. Angew. Chem., Int. Ed. 2018, 57, 10656.
(11) Brunsveld, L.; Folmer, B. J. B.; Meijer, E. W.; Sijbesma, R. P. Supramolecular Polymers. Chem. Rev. 2001, 101, 4071−4098.
(12) El-Hachemi, Z.; Escudero, C.; Acosta-Reyes, F.; Casas, M. T.; Altoe, V.; Aloni, S.; Oncins, G.; Sorrenti, A.; Crusats, J.; Campos, J. L.; Ribó, J. M. Structure vs. properties - chirality, optics and shapes - in amphiphilic porphyrin J-aggregates. J. Mater. Chem. C 2013, 1, 3337−3346.
(13) Yang, Y.; Walz, J.; Pintauro, P. Curvature effects on electric double-layer forces. Part 1.-Comparisions with parallel geometry. J. Chem. Soc. Faraday Trans. 1995, 91, 2827−2836.
(14) May, S. Curvature elasticity and thermodynamic stability of electrically charged membranes. J. Chem. Phys. 1996, 105, 8314−8323.
(15) Yang, Y.; Walz, J.; Pintauro, P. Curvature effects on electric double-layer forces Part 2.-Dependence of forces on cavity radius and the relative permittivity. J. Chem. Soc. Faraday Trans. 1997, 93, 603−611.
(16) Escudero, C.; El-Hachemi, Z.; Crusats, J.; Ribó, J. M. Zwitterionic vs Porphyrin Free-Base Structures in 4-Phenylsulfonic Acid Meso-Substituted Porphyrins. J. Porphyrin Phtalocyanines 2005, 9, 852−863.
(17) Rahman, M.; James Harmon, H. Inhibition of aggregation of meso-tetra(4-sulfonatophenyl)-porphyrin (H$_4$TPPS) by urea. J. Porphyrins Phthalocyanines 2007, 11, 125−129.
(18) Purrello, R.; Bellacchio, E.; Gurrieri, S.; Lauceri, R.; Raudino, A.; Scolaro, L. M.; Santoro, A. M. pH Modulation of Porphyrins Self-Assembly onto Polylysine. J. Phys. Chem. B 1998, 102, 8852−8857.

(19) Lauceri, R.; Campagna, T.; Raudino, A.; Purrello, R. Porphyrin Binding and Self-Aggregation onto Polymeric Matrix: A Combined Spectroscopic and Modelling Approach. *Inorg. Chim. Acta* **2001**, *317*, 282−289.

(20) De Luca, G.; Romeo, A.; Scolaro, L. M.; Pasternack, R. F. Conformations of a Model Protein Revealed by an Aggregating CuII Porphyrin: Sensing the Difference. *Chem. Commun.* **2010**, *46*, 389−391.

(21) Wang, Z.; Medforth, C. J.; Shelnutt, J. A. Porphyrin Nanotubes by Ionic Self-Assembly. *J. Am. Chem. Soc.* **2004**, *126*, 15954−15955.

(22) Friesen, B. A.; Rich, C. C.; Mazur, U.; McHale, J. L. Resonance Raman Spectroscopy of Helical Porphyrin Nanotubes. *J. Phys. Chem. C* **2010**, *114*, 16357−16366.

(23) Philip, J. R.; Wooding, R. A. Solution of the Poisson-Boltzmann Equation about a Cylindrical Particle. *J. Chem. Phys.* **1970**, *52*, 953−959.

(24) Arteaga, O.; Canillas, A.; El-Hachemi, Z.; Crusats, J.; Ribó, J. M. Structure vs. Excitonic Transitions in Self-Assembled Porphyrin Nanotubes and their Effect on Light Absorption And Scattering. *Nanoscale* **2015**, *7*, 20435−20441.

(25) Rubires, R.; Crusats, J.; El-Hachemi, Z.; Jaramillo, T.; López, M.; Valls, E.; Farrera, J.-A.; Ribó, J. M. Self-Assembly in Water of the Sodium Salts of *meso*-Sulfonatophenyl Substituted Porphyrins. *New J. Chem.* **1999**, *23*, 189−198.

(26) García-Ortega, H. Porfirinas Solubles en Agua: Síntesis, Homoasociación y Propiedades Fotofísicas de Porfirinas Sulfonadas 5,15-Difenilsustituidas. PhD Thesis, University of Barcelona, Faculty of Chemistry, 2003.

(27) Escudero, C.; Crusats, J.; Díez-Pérez, I.; El-Hachemi, Z.; Ribó, J. M. Folding and Hydrodynamic Forces in J-Aggregates of 5-Phenyl-10,15,20-tris(4-sulfophenyl)porphyrin. *Angew. Chem., Int. Ed.* **2006**, *45*, 8032−8035.

(28) Sorrenti, A.; El-Hachemi, Z.; Crusats, J.; Ribo, J. M. Effects of Flow-Selectivity on Self-Assembly and Auto-Organization Processes: An Example. *Chem. Commun.* **2011**, *47*, 8551−8553.

(29) Short, J. M.; Berriman, J. A.; Kübel, C.; El-Hachemi, Z.; Naubron, J.-V.; Balaban, T. S. Electron Cryo-Microscopy of TPPS₄· 2HCl Tubes Reveals a Helical Organisation Explaining the Origin of their Chirality. *ChemPhysChem* **2013**, *14*, 3209−3214.

(30) Ribo, J. M.; Crusats, J.; Sagués, F.; Claret, J.; Rubires, R. Chiral Sign Induction by Vortices During the Formation of Mesophases in Stirred Solutions. *Science* **2001**, *292*, 2063−2066.

(31) El-Hachemi, Z.; Escudero, C.; Arteaga, O.; Canillas, A.; Crusats, J.; Mancini, G.; Purrello, R.; Sorrenti, A.; D'Urso, A.; Ribo, J. M. Chiral Sign Selection on the J-Aggregates of Diprotonated Tetrakis-(4-Sulfonatophenyl)Porphyrin by Traces of Unidentified Chiral Contaminants Present in the Ultra-Pure Water Used As Solvent. *Chirality* **2009**, *21*, 408−412.

(32) Micali, N.; Engelkamp, H.; van Rhee, P. G.; Christianen, P. C. M.; Scolaro, L. M.; Maan, J. C. Selection of Supramolecular Chirality by Application of Rotational and Magnetic Forces. *Nat. Chem.* **2012**, *4*, 201−207.

(33) Sun, J.; Li, Y.; Yan, F.; Liu, C.; Sang, Y.; Tian, F.; Feng, Q.; Duan, P.; Zhang, L.; Shi, X.; Ding, B.; Liu, M. Control Over the Emerging Chirality in Supramolecular Gels and Solutions by Chiral Microvortices in Milliseconds. *Nat. Commun.* **2018**, *9*, 2599.

(34) McBride, J. M.; Carter, R. L. Spontaneous Resolution by Stirred Crystallization. *Angew. Chem., Int. Ed. Engl.* **1991**, *30*, 293−295.

(35) Zurita, A.; Duran, A.; Ribó, J. M.; El-Hachemi, Z.; Crusats, J. Hyperporphyrin Effects Extended into a J-Aggregate Supramolecular Structure in Water. *RSC Adv.* **2017**, *7*, 3353−3357.

(36) Zhu, J.; Hayward, R. C. Spontaneous Generation of Amphiphilic Block Copolymer Micelles with Multiple Morphologies through Interfacial Instabilities. *J. Am. Chem. Soc.* **2008**, *130*, 7496−7502.

(37) Cukierman, S. Et tu, Grotthuss! and other unfinished stories. *Biochim. Biophys. Acta* **2006**, *1757*, 876−885.

(38) Ribó, J. M.; Blanco, C.; Crusats, J.; El-Hachemi, Z.; Hochberg, D.; Moyano, A. Absolute Asymmetric Synthesis in Enantioslective

Autocatalytic Reaction Networks. *Chem.—Eur. J.* **2014**, *20*, 17250−17271.

(39) Guo, P.; Chen, P.; Ma, W.; Liu, M. Morphology-Dependent Supramolecular Photocatalytic Performance of Porphyrin Nano-assemblies: From Molecule to Artificial Supramolecular Nanoantenna. *J. Mater. Chem.* **2012**, *22*, 20243−20249.

(40) McHale, J. L. Hierarchal Light-Harvesting Aggregates and their Potential for Solar Energy Applications. *J. Phys. Chem. Lett.* **2012**, *3*, 587−597.

(41) Po, H. N.; Senozan, N. M. The Henderson-Hasselbalch Equation: Its History and Limitations. *J. Chem. Educ.* **2001**, *78*, 1499.

(42) Ercolani, G.; Ioele, M.; Monti, D. Physical Basis of Self-Assembly. Part 2. A Theoretical and Experimental Study of the Self-Assembly of a Zinc Meso-Pyridyl Porphyrin. *New J. Chem.* **2001**, *25*, 783−789.

(43) Koszarna, B.; Gryko, D. T. Efficient Synthesis of meso-Substituted Corroles in a H₂O−MeOH Mixture. *J. Org. Chem.* **2006**, *71*, 3707−3717.

(44) Littler, B. J.; Miller, M. A.; Hung, C.-H.; Wagner, R. W.; O'Shea, D. F.; Boyle, P. D.; Lindsey, J. S. Refined Synthesis of 5-Substituted Dipyrromethanes. *J. Org. Chem.* **1999**, *64*, 1391−1396.